PROCEEDINGS, 42nd Workshop on Geothermal Reservoir Engineering
Stanford University, Stanford, California, February 13-15, 2017
SGP-TR-212

Anisotropic Reverse-Time Migration for Imaging Fracture Zones at Eleven-Mile Canyon

Miao Zhang, Kai Gao and Lianjie Huang

Los Alamos National Laboratory, Los Alamos, NM 87545, USA

Emails: mzhang@lanl.gov, kaigao@lanl.gov, ljh@lanl.gov

Keywords: Anisotropic Reverse-time Migration, Eleven-Mile Canyon, Fracture Zone, Geothermal, Seismic Imaging

ABSTRACT

Fracture zones behave as anisotropic media for seismic-wave propagation. Conventional reverse-time migration is based on seismic-wave propagation in isotropic media, and usually fails to reliably image fracture/fault zones for geothermal exploration. We develop a novel anisotropic reverse-time migration method for reliable imaging of fracture zones. The method employs an implicit wavefield separation scheme to properly handle arbitrary anisotropy of fracture zones. We validate our new method using synthetic data for a geophysical models of Eleven-Mile Canyon in Nevada containing several fracture zones. The synthetic test results show that our new method produce higher-quality images of fracture zones than the conventional RTM. Several 2D surface seismic reflection datasets were acquired at Eleven-Mile Canyon in Nevada for geothermal exploration. We update velocity model of a 2D-line seismic data using envelope-correlation-based full waveform inversion. We apply our new anisotropic reverse-time migration method to the 2D-line seismic data to image subsurface structures at Eleven-Mile Canyon geothermal exploration site. Our preliminary imaging results of field seismic data demonstrate the effectiveness of our new anisotropic reverse-time migration method for imaging complex structures in anisotropic media such as fracture zones.

1. INTRODUCTION

The Eleven-Mile Canyon geothermal exploration field is located near the margins of Dixie Valley, a NNE-SSW-trending late Cenozoic structural basin, 100 kilometers east of Fallon, Nevada. It is close to the surface rupture terminations of 1954 Fairview Peak – Dixie Valley earthquake sequence (Alm et al., 2016). This geothermal field in Dixie Valley contains a complex network of faults and fractures consisting of steep dips, which creates the highly permeable fractures for the production zone at 2-3 kilometers in depth (Unruh et al., 2016). It is important to image the subsurface fracture zones for interpretations of the extensional structure generating heat flow capacity in the geothermal system. Five 2D seismic reflection lines were conducted in 2013 to evaluate geothermal potential at Eleven-Mile Canyon in southern Dixie Valley, Nevada.

Fracture zones may provide paths for hydrothermal flow, but they may also be effective barriers to geothermal flow in some situations (Ba et al., 2015). Fracture identification and characterization is crucial for geothermal exploration and optimizing enhanced geothermal systems. However, it is particular challenging to image fracture zones because of complicated heterogeneities and possible anisotropies in both fracture zones and surrounding rocks.

Reverse time migration (RTM) is the most powerful tool for imaging complex subsurface structures. RTM solves acoustic-/elastic-wave equations for wavefield extrapolation and has no dip limitations. In addition, RTM is also able to handle arbitrary types of subsurface media. In conventional RTM methods, the elastic medium is widely assumed to be isotropic. However, most crustal rocks are found experimentally to be anisotropic. In some particular geological area, the anisotropy is as strong as 20%, or even larger. The imaged fractures could be wrongly positioned or totally missing using conventional RTM based on the isotropic assumption. By assuming the weak anisotropy of elastic media, acoustic approximations have been used to describe the anisotropy using Thomsen parameters and reference velocity values (Thomsen, 1986; Plessix and Cao, 2011).

We have recently developed a new anisotropic reverse-time migration method (anisotropic RTM) using the parameterization of elasticity constants in anisotropic media. An implicit wavefield separation scheme is employed to properly handle arbitrary anisotropy of fracture zones. Our anisotropic RTM is able to handle complicated anisotropy such as transversely isotropy with titled symmetric axis (TTI) or monoclinic anisotropy in fractured zones.

In this paper, we first validate the effectiveness of our anisotropic RTM method using synthetic data for a geophysical model of the Eleven-Mile Canyon geothermal exploration site by comparing the results with those obtained with the conventional isotropic RTM. Then we apply our new anisotropic RTM to a 2D line of surface seismic reflection data acquired at Eleven-Mile Canyon, and compare the image with that obtained using isotropic RTM.

2. ANISOTROPIC RESERVE-TIME MIGRATION

We briefly review the anisotropic reverse-time migration method. The forward modeling of elastic-wave propagation in anisotropic media is based on velocity-stress equations given by (Gao et al., 2015; Gao and Huang, 2015)

$$\frac{\partial \sigma}{\partial t} = C\Lambda^T v, \quad \frac{\partial v}{\partial t} = \rho^{-1}\Lambda\sigma, \tag{1}$$

where $\sigma=(\sigma_{11},\sigma_{33},\sigma_{13})$ is the stress wavefield, $v=(v_1,v_3)$ is the particle velocity wavefield, ρ is the mass density of the medium, C is the elastic tensor in Voigt notation defined as

$$C=\begin{pmatrix} C_{11} & C_{13} & C_{15} \\ C_{13} & C_{33} & C_{35} \\ C_{15} & C_{35} & C_{55} \end{pmatrix}, \tag{2}$$

and Λ is the differential operator defined as

$$\Lambda=\begin{pmatrix} \frac{\partial}{\partial x_1} & 0 & \frac{\partial}{\partial x_3} \\ 0 & \frac{\partial}{\partial x_3} & \frac{\partial}{\partial x_1} \end{pmatrix}. \tag{3}$$

In anisotropic media, separation of qP- and qS-wave is known to be more complicated and more computationally expensive than that in isotropic media. We adopt a nonstationary spatial filtering method to achieve the complete separation of qP- and qS-wavefield components in heterogeneous medium (Yan and Sava, 2009):

$$qP=\nabla_a\cdot U,\ qS=\nabla_a\times U, \tag{4}$$

where ∇_a are the pseudo-derivative operators in space, and they should be solved using the Christoffel equation for anisotropic media at every space location.

To obtain the imaging conditions for anisotropic RTM, we decompose the source and receiver wavefileds into their directional components, and we can also further decompose the wavefields along left and right directions (Fei et al., 2015).

The down-going anisotropic RTM image can be obtained using

$$I_{\text{pp,down}}(\mathbf{x})=\sum_{N_s,N_r}\int_0^T[P_sP_r-H_z(P_s)H_z(P_r)-P_sH_z(H_t(P_r))-H_z(P_s)H_t(P_r)]dt,$$

$$I_{\text{ps,down}}(\mathbf{x})=\sum_{N_s,N_r}\int_0^T[P_sS_r-H_z(P_s)H_z(S_r)-P_sH_z(H_t(S_r))-H_z(P_s)H_t(S_r)]dt, \tag{5}$$

where s and r represent the source and receiver wavefield, respectively, P and S indicate separated qP- and qS-wavefields calculated using equation (4), H_z represents the Hilbert transform in the vertical direction, and H_t represents the Hilbert transform in the time domain.

Similarly, the left-going and right-going images are generated using

$$I_{\text{pp,left}}(\mathrm{x})=\sum_{N_s,N_r}\int_0^T[P_sP_r-H_x(P_s)H_x(P_r)-P_sH_x(H_t(P_r))-H_x(P_s)H_t(P_r)]dt,$$

$$I_{\text{ps,left}}(\mathrm{x})=\sum_{N_s,N_r}\int_0^T[P_sS_r-H_x(P_s)H_x(S_r)-P_sH_x(H_t(S_r))-H_x(P_s)H_t(S_r)]dt, \tag{6}$$

and

$$I_{\text{pp,right}}(\mathrm{x})=\sum_{N_s,N_r}\int_0^T[P_sP_r-H_x(P_s)H_x(P_r)-P_sH_x(H_t(P_r))-H_x(P_s)H_t(P_r)]dt,$$

$$I_{\text{ps,right}}(\mathrm{x})=\sum_{N_s,N_r}\int_0^T[P_sS_r-H_x(P_s)H_x(S_r)-P_sH_x(H_t(S_r))-H_x(P_s)H_t(S_r)]dt, \tag{7}$$

respectively, where H_x represent the Hilbert transform in the horizontal direction.

3. SYNTHETIC TESTS

We apply our anisotropic RTM method to synthetic seismic data for a geophysical model of Eleven-Mile Canyon. The model contains several anisotropic fracture zones. We first build isotropic Vp and Vs models based on local geological information and lithostratigraphic information (Fig. 1). We assume that the subsurface medium behaves vertical transverse isotropy (VTI) and wave propagation along the horizontal direction is 20% faster than that along the vertical direction. The constructed fracture zones behave tilted transverse isotropic (TTI) property. The fracture zones have low velocity values for both Vp and Vs. The qP- and qS-velocity are 20% and 10% faster along the fracture zones than those in their surrounding media for large fracture zones and small fractures, respectively (Fig. 2). The constructed six anisotropic parameters are shown in Fig. 2. We generate synthetic surface seismic reflection data using these anisotropic parameters for 240 shots and 249 receivers with the same source-receiver configuration as the field seismic data acquisition in 2013.

We conduct conventional isotropic RTM using the isotropic Vp and Vs models and perform anisotropic RTM using anisotropic models without fracture zones, respectively. The conventional RTM images are blurred and unfocused because of incorrect velocity model (Fig. 3). In contrast, our anisotropic RTM results clearly image these fracture zones (Fig. 4). These synthetic test results demonstrate that our new anisotropic RTM method produces higher-quality images of fracture zones than the conventional isotropic RTM.

4. APPLICATION TO FIELD SEISMIC DATA

We apply isotropic RTM and anisotropic RTM to a 2D line of surface seismic data acquired at Eleven-Mile Canyon in 2013. We assume the subsurface media contain weak anisotropy described using Thomsen parameters. Only the vertical component of seismic data was acquired in the seismic reflection survey at Eleven-Mile Canyon. We first remove dead traces from the original data. For 2D migration imaging, each trace is multiplied by $\sqrt{i/\omega}$ in the frequency domain, where i is the imaginary unit and ω is the angular frequency, and then scaled by $\sqrt{t}$ in the time domain with time t to correct for the 3D geometrical spreading. We remove the ground roll noise in the seismic data before using them for migration and inversion (Fig. 5). The initial velocity model is smoothed from the result of refraction tomography (Fig. 6a). The anisotropic RTM yields more clear and continuous images compared to those obtained using isotropic RTM (Fig. 7). We update the isotropic velocity model using envelope-correlation-based full-waveform inversion method (Fig. 6b). Figure 8 shows that some reflectors in the isotropic and anisotropic RTM images obtained using the updated velocity model seem to be more continuous than those in Fig. 7. The zoomed image comparison between Fig. 7 and Fig. 8 is shown in Fig. 9. The possible fracture/fault zones can be clearly identified in the anisotropic RTM images, but they are almost invisible in isotropic RTM images (Fig. 9). The identified fracture zones may be consistent with the geological information at Eleven-Mile Canyon as shown in Fig. 2.

5. CONCLUSIONS

We have validated our newly developed anisotropic reverse-time migration method using synthetic seismic data for a seismic velocity model of Eleven-Mile Canyon at Dixie Valley in Nevada. The model contains several fracture zones with anisotropic properties. Our anisotropic reverse-time migration produces clear images of fracture zones with much fewer image artifacts than those obtained using isotropic reverse-time migration. We have applied our anisotropic acoustic reverse-time migration method to a 2D line of seismic data acquired at Eleven-Mile Canyon. Our results demonstrate that it is essential to properly account for anisotropic properties for fracture imaging.

6. ACKNOWLEDGEMENTS

This work was supported by the Geothermal Technologies Office (GTO) of the U.S. Department of Energy through contract DE-AC52-06NA25396 to Los Alamos National Laboratory (LANL). We thank strong support of GTO Program Managers Eric Hass, Holly Thomas, and Brittany Segneri. We thank Andrew Sabin of the US Navy Geothermal Program Office for providing the field seismic data from Eleven-Mile Canyon. We acknowledge Yunsong Huang of LANL for data processing to remove ground roll noise. The computation was performed on super-computers provided by the Institutional Computing Program of Los Alamos National Laboratory.

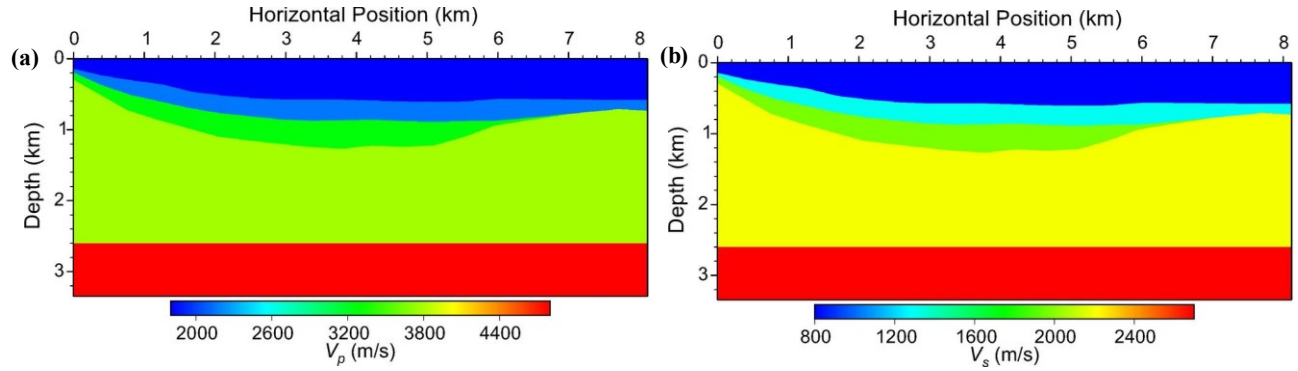

Figure 1: Vp and Vs models used for isotropic reverse-time migration.

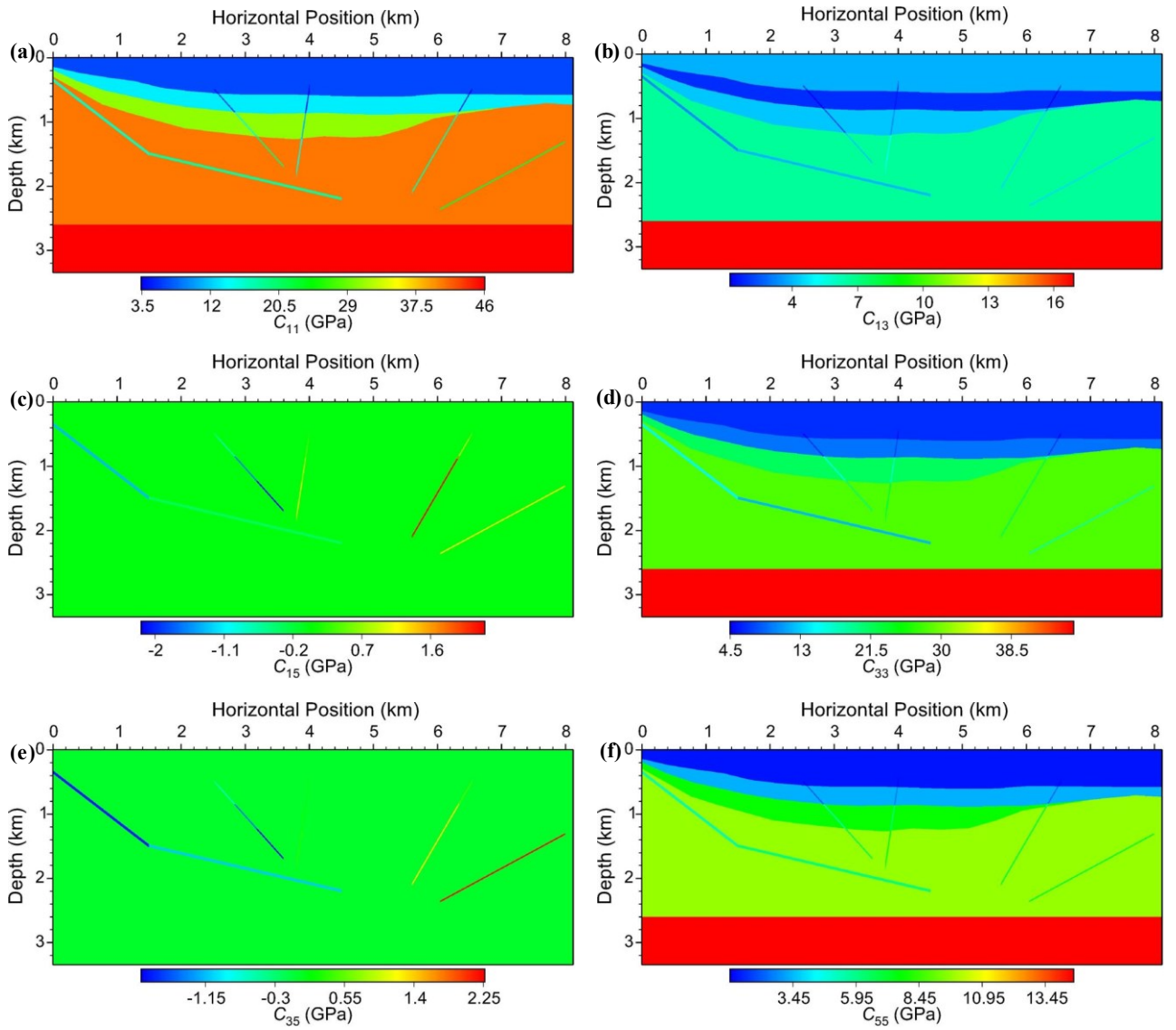

Figure 2: Six anisotropic parameters used for anisotropic RTM. The surrounding velocities behave VTI properties. The model contains five TTI fracture zones.

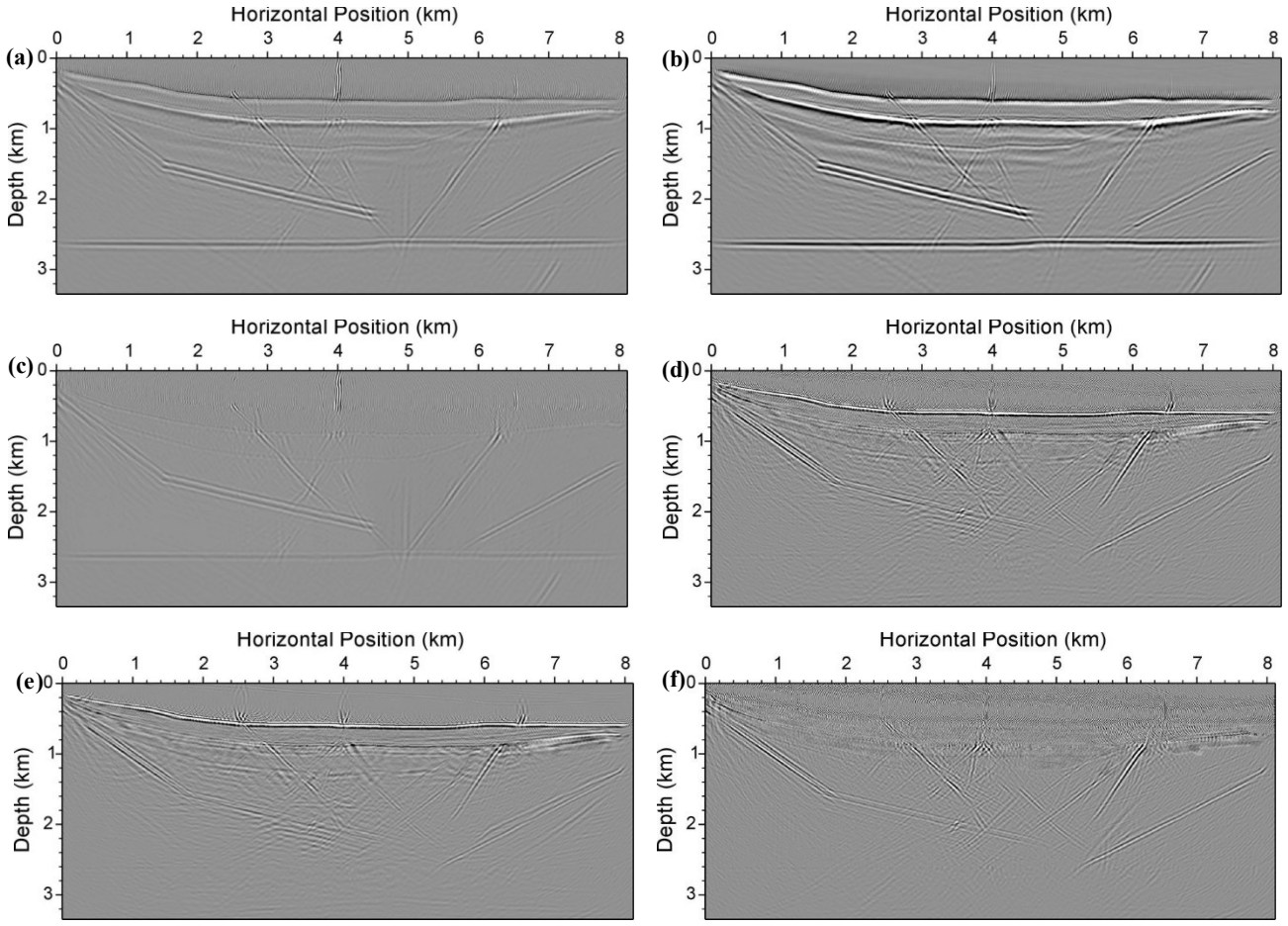

Figure 3: Isotropic RTM images obtained using the velocity model in Fig. 1 and synthetic data for the model in Fig. 2. (a) Total PP image, (b) downward-looking PP image, (c) horizontal-looking PP image, (d) total PS image, (e) PS downward-looking image, (f) horizontal-looking PS image.

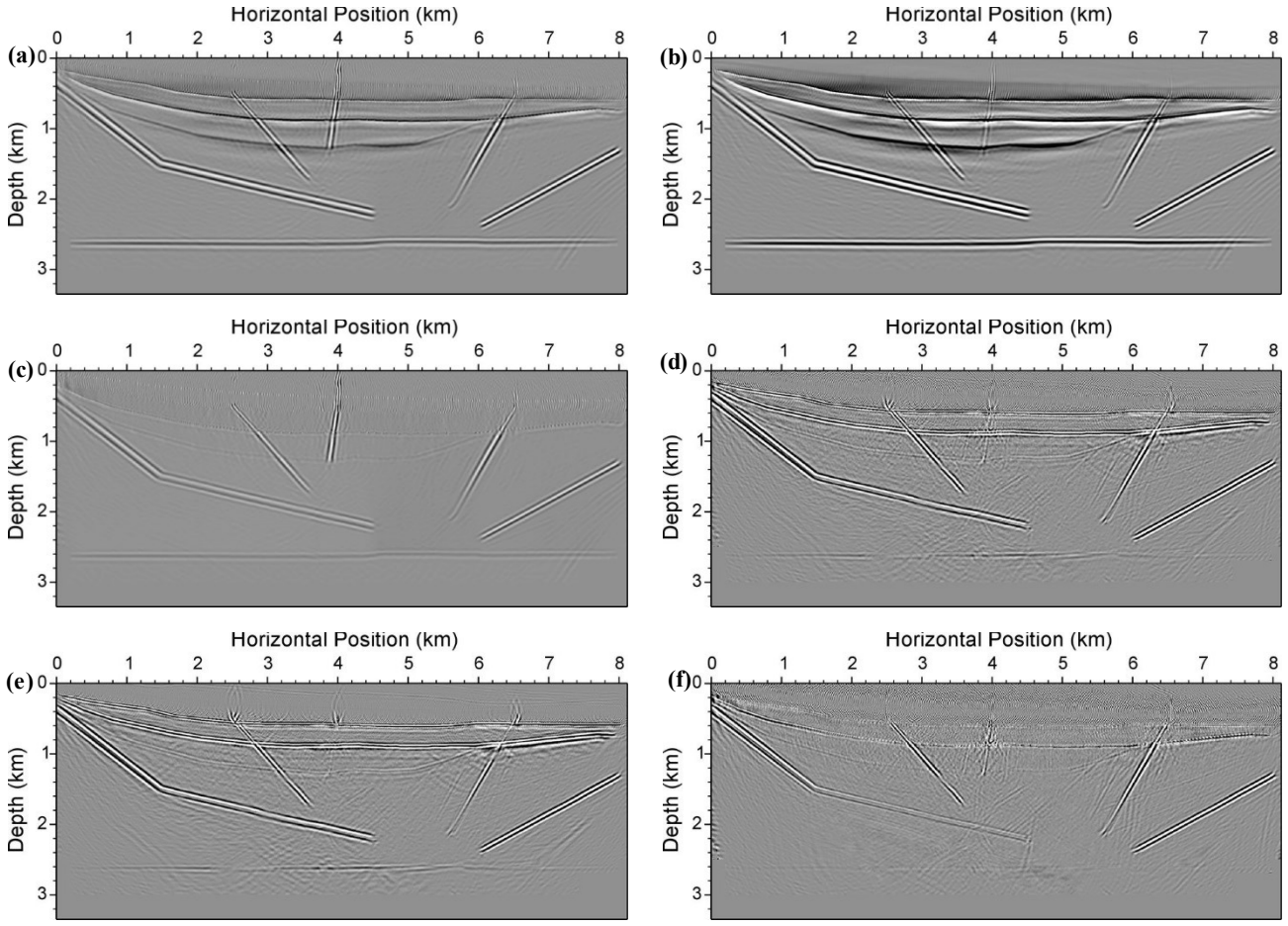

Figure 4: Anisotropic RTM images obtained using synthetic data for the model in Fig. 2. (a) Total PP image, (b) downward-looking PP image, (c) horizontal-looking PP image, (d) total PS image, (e) PS downward-looking image, (f) horizontal-looking PS image.

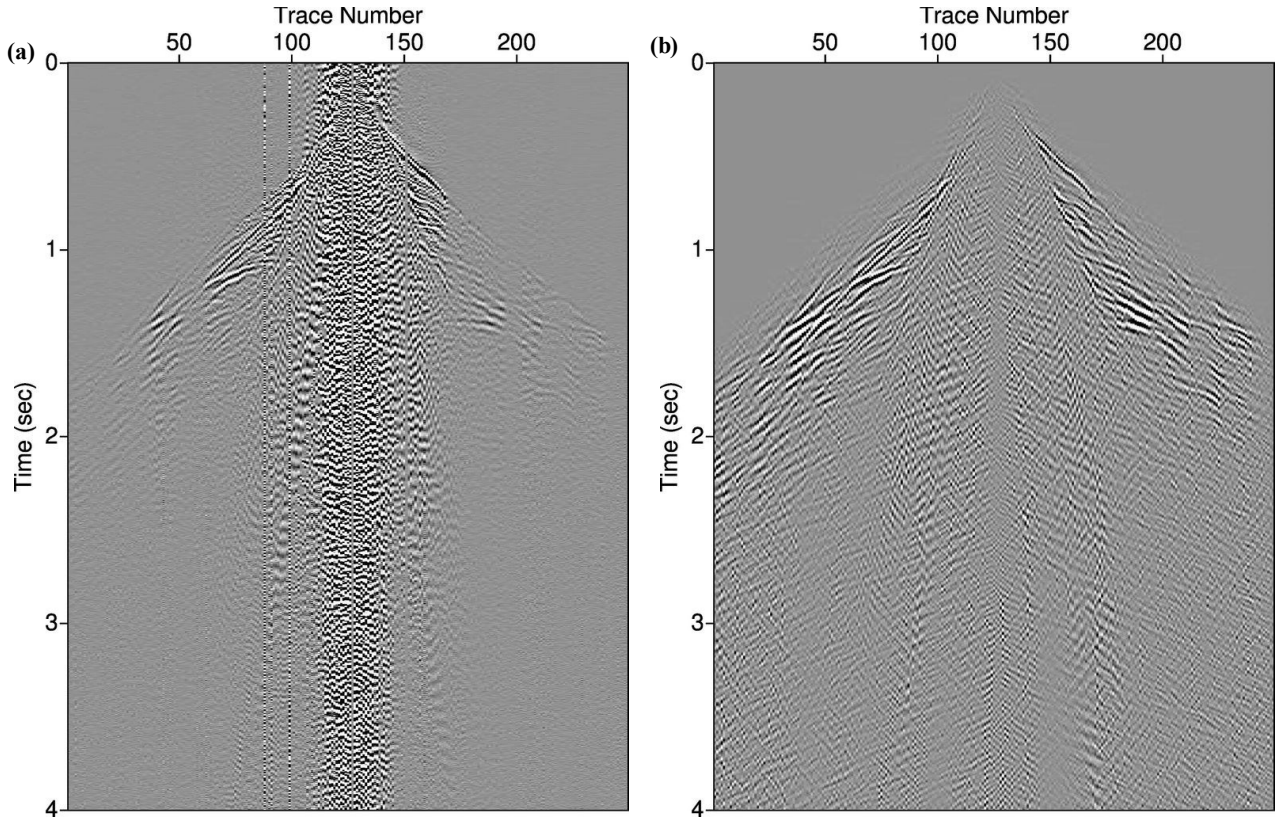

Figure 5: Waveform comparison of a common-shot gather before and after data processing (removing dead traces, bandpass filtering, trace balancing, geometrical spreading correction, and removing the ground roll noise).

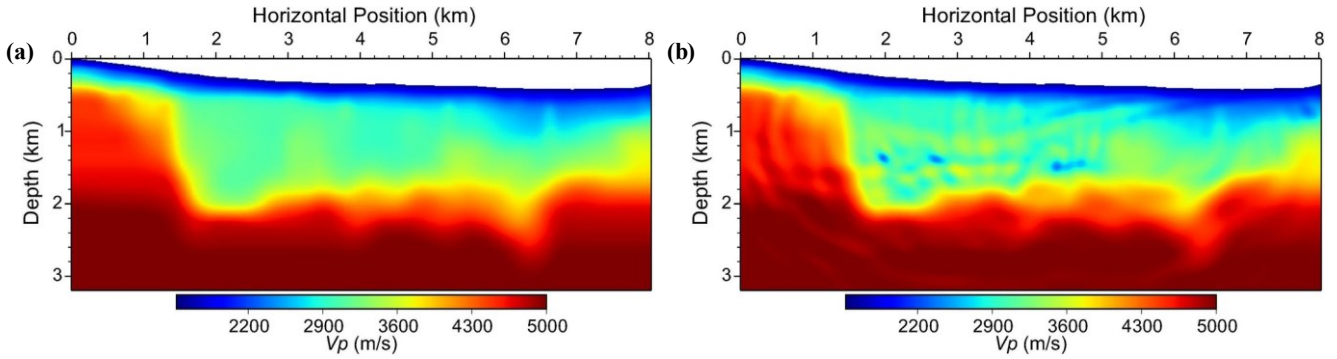

Figure 6: Initial velocity model from refraction tomography (a) and updated velocity model inverted using full-waveform inversion (b).

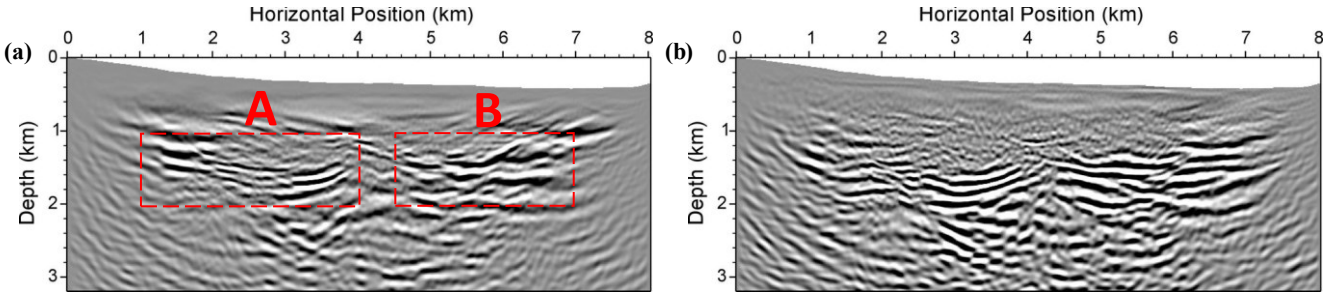

Figure 7: Isotropic RTM (a) and anisotropic RTM (b) images obtained using Line 1 seismic data from Eleven-Mile Canyon and the initial velocity model in Fig. 6a. The zoomed images in regions A and B are shown in Fig. 9.

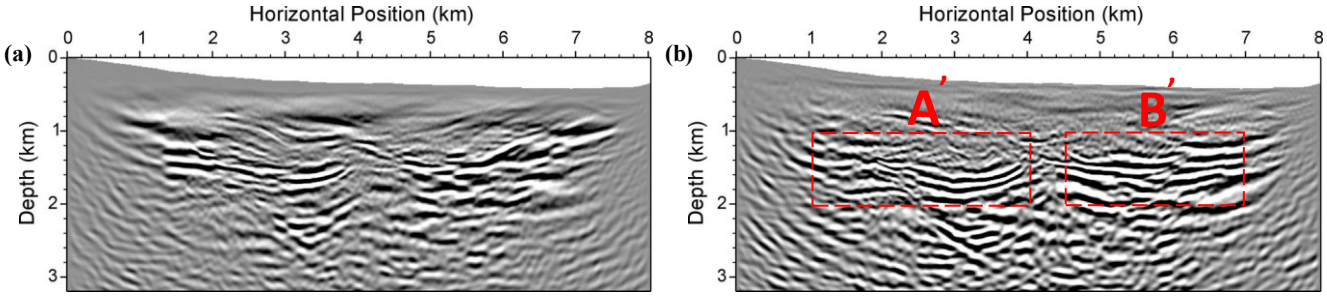

Figure 8: Isotropic RTM (a) and anisotropic RTM (b) images obtained using Line 1 seismic data from Eleven-Mile Canyon and the updated velocity model inverted with full-waveform inversion in Fig. 6b. The zoomed images in regions A and B are shown in Fig. 9.

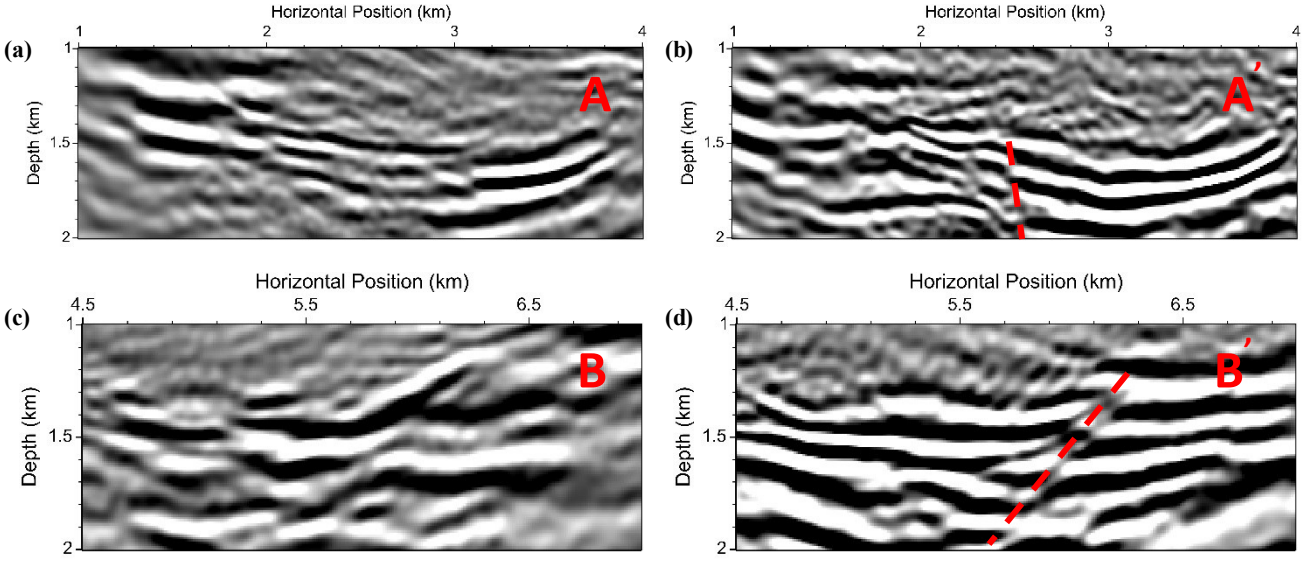

Figure 9: Comparison of the zoomed images in regions A and B in Fig. 7 and Fig. 8. State-of-the-art isotropic RTM images (a, c) using initial velocity model, and anisotropic RTM (b, d) images using the updated velocity model inverted using full-waveform inversion. The possible fracture/fault zones around the red dashed lines in (b, d) are not clearly imaged in (a, c).

REFERENCES

Alm, S., Walker, J.D., and Blake, K.: Structural complexity of the Pirouette Mountain and Elevenmile Canyon Geothermal Systems, *Transactions, Geothermal Resources Council*, **40**, (2016), 433-438.

Ba, J., Du, Q., Carcione, J.M., Zhang, H., and Muller, T.M.: Seismic exploration of hydrocarbons in heterogeneous reservoirs, first ed.: Elsevier (2015).

Gao, K., Lin, Y., Huang, L., Queen, J., Moore, J., and Majer, E.: Anisotropic elastic waveform inversion with modified total-variation regularization, *SEG Technical Program Expanded Abstracts* 2015, (2015).

Gao, K., and Huang, L.: Anisotropic Elastic-Waveform Modeling for Fracture Characterization in EGS Reservoirs, *Proceedings,* 40th Workshop on Geothermal Reservoir Engineering, Stanford University, Stanford, CA (2015).

Fei, T., Luo, Y., Yang, J., Liu H., and Qin, F.: Removing false images in reverse time migration: The concept of de-primary, *Geophysics*, **80**(5), S237-S244.

Plessix, R.E., and Cao, Q.: A parametrization study for surface seismic full waveform inversion in an acoustic vertical transversely isotropic medium, *Geophysical Journal International*, **185**, (2011), 539-556.

Thomsen, L.: Weak elastic anisotropy, *Geophysics*, **51**, (1986), 1954-1966.

Unruh, J., Gray, B., Christopherson, K., Pullammanappallil, S., Alm, S., and Blake, K.: Seismic Reflection and Magnetotelluric Imaging of Southwestern Dixie Valley Basin, Nevada, *Transactions, Geothermal Resources Council*, **40**, (2016), 455-461.

Yan, J., and Sava, P.: Elastic wave-mode separation for VTI media, Geophysics, **74**(5), (2009), WB19-WB32.